

SOFT ROBOTS

Peano-HASEL actuators: Muscle-mimetic, electrohydraulic transducers that linearly contract on activation

Nicholas Kellaris,^{1,2} Vidyacharan Gopaluni Venkata,¹ Garrett M. Smith,¹
Shane K. Mitchell,¹ Christoph Keplinger^{1,2*}

Copyright © 2018
The Authors, some
rights reserved;
exclusive licensee
American Association
for the Advancement
of Science. No claim
to original U.S.
Government Works

Soft robotic systems are well suited to unstructured, dynamic tasks and environments, owing to their ability to adapt and conform without damaging themselves or their surroundings. These abilities are crucial in areas such as human-robot interaction. Soft robotic systems are currently limited by the soft actuators that power them. To date, most soft actuators are based on pneumatics or shape-memory alloys, which have issues with efficiency, response speed, and portability. Dielectric elastomer actuators (DEAs) are controlled and powered electrically and excel with muscle-like actuation, but they typically require a rigid frame and prestretch to perform effectively. In addition, DEAs require complex stacks or structures to achieve linear contraction modes. We present a class of soft electrohydraulic transducers, termed Peano-HASEL (hydraulically amplified self-healing electrostatic) actuators, that combine the strengths of fluidic actuators and electrostatic actuators, while addressing many of their issues. These actuators use both electrostatic and hydraulic principles to linearly contract on application of voltage in a muscle-like fashion, without rigid frames, prestretch, or stacked configurations. We fabricated these actuators using a facile heat-sealing method with inexpensive commercially available materials. These prototypical devices demonstrated controllable linear contraction up to 10%, a strain rate of 900% per second, actuation at 50 hertz, and the ability to lift more than 200 times their weight. In addition, these actuators featured characteristics such as high optical transparency and the ability to self-sense their deformation state. Hence, this class of actuators demonstrates promise for applications such as active prostheses, medical and industrial automation, and autonomous robotic devices.

INTRODUCTION

Traditional mechanical systems, made from rigid components such as pistons and electromagnetic motors, excel at precise and repetitive tasks. As a result, these rigid systems have seen widespread application in areas such as industrial automation. However, they have limited adaptability, which restricts their effectiveness in unstructured and dynamic environments. Soft robotic systems, which are based on compliant materials and structures, demonstrate promise in these unpredictable situations due to their resilience, adaptability, and shock-absorbing characteristics (1–6).

Soft actuators currently explored for use in robotic systems are numerous [Hines *et al.* (7) provides a good overview of various soft actuator technologies] and include thermally responsive polymers (8), fluidic actuators (both pneumatic and hydraulic) (9–15), and dielectric elastomer actuators (DEAs) (16–19). Of these, pneumatic actuators are the most prevalent because they can achieve high actuation force and large strokes, similar to natural muscle (20). In addition, they are highly versatile, which allows them to achieve varied modes of actuation (21). However, pneumatic actuators have low efficiency (11) and experience substantial trade-offs between actuation speed and portability, with the response speed of untethered devices being low (2, 22); high-power operation requires rigid and bulky reservoirs or compressors.

Electrically powered actuators, such as DEAs, offer several advantages such as high-speed actuation, high strain (>100%) (16), silent operation, and self-sensing (23). However, DEAs are driven by high electric fields, which can lead to irreversible dielectric breakdown. The likelihood of

dielectric failure, which follows Weibull statistics, increases as electrode area is scaled up (24), reducing the reliability of DEAs for large-scale applications. Furthermore, DEAs typically require rigid and bulky frames to provide a prestretch for high-strain and high-power operation, with current freestanding DEAs limited to small strains (25–27). In addition, actuation modes are generally limited to elongation on activation, with contraction being achieved through stacked configurations (28) that require elaborate fabrication processes and large electrode areas, increasing risk of dielectric failure.

Here, we introduce Peano-HASEL actuators as a class of versatile, soft electrohydraulic transducers that feature fast linear contraction on activation, demonstrate high force production and scalability, and can be made from inexpensive materials that are compatible with industrial fabrication methods. Peano-HASEL actuators synergize the strengths of linearly contracting Peano fluidic actuators created by Niiyama *et al.* (12) and Sanan *et al.* (13), and hydraulically amplified self-healing electrostatic (HASEL) actuators recently developed by Acome *et al.* (29). Building upon the fundamental physical concepts of HASEL actuators introduced in (29), Peano-HASEL actuators use a materials system based on inextensible but flexible thin shells, thereby eliminating the need for highly stretchable electrodes and dielectrics. Peano-HASELs have several distinctive qualities: (i) They linearly contract on application of voltage without relying on prestretch, rigid frames, or stacked configurations; (ii) they are electrically powered, which grants them the advantages of DEAs such as high-speed operation and the ability to self-sense their deformation state through capacitance monitoring (23); (iii) they incorporate a liquid dielectric, which provides direct coupling of electrostatic and hydraulic forces for high-power and precise operation, without requiring external sources of compressed fluids or pumps; (iv) they can be made from a variety of materials, even allowing for highly transparent

¹Department of Mechanical Engineering, University of Colorado Boulder, Boulder, CO 80309, USA. ²Materials Science and Engineering Program, University of Colorado Boulder, Boulder, CO 80309, USA.

*Corresponding author. Email: christoph.keplinger@colorado.edu

designs; and (v) they are fabricated using industrially compatible methods such as heat sealing.

RESULTS

Principles of operation and design

Peano-HASEL actuators operate on electrostatic and hydraulic principles, as shown in Fig. 1A. The actuator consists of a series of rectan-

gular pouches made from a flexible and inextensible shell that is filled with a liquid dielectric. Electrodes cover a portion of each pouch on either side of the actuator. When a voltage is applied, electrostatic forces displace the liquid dielectric, causing the electrodes to progressively close, such as in electrostatic “zipping” actuators (30–33). These electrostatic forces are determined by the Maxwell pressure, $P \propto \epsilon E^2$ (34), where ϵ is the dielectric permittivity and E is the magnitude of the electrical field. This pressure forces fluid into the uncovered portion

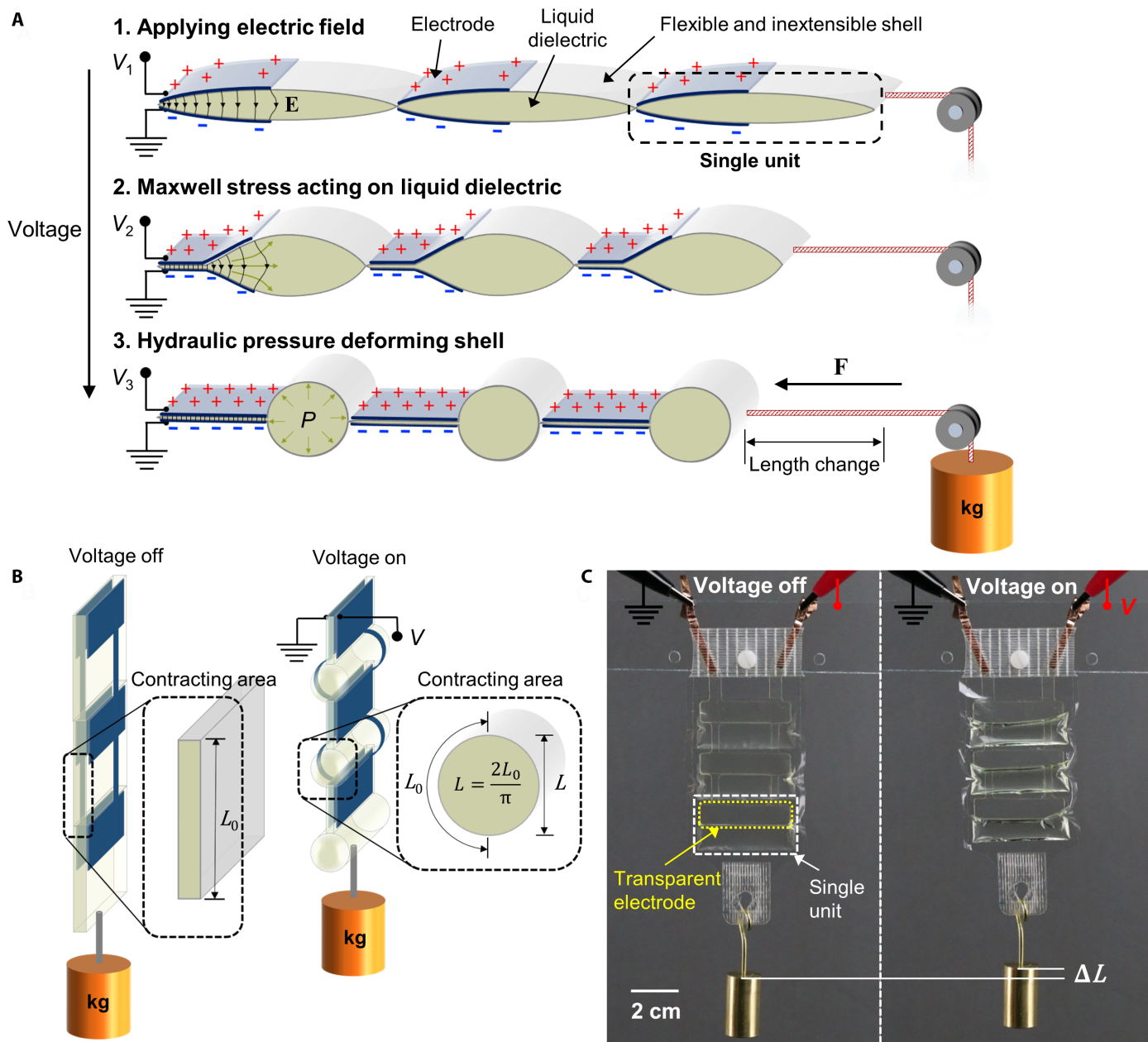


Fig. 1. Basic components of Peano-HASEL actuators and principles of operation. (A) Schematic side view showing the cross section of a three-unit Peano-HASEL actuator; each unit consists of a rectangular pouch made from an inextensible and flexible polymer shell, filled with a liquid dielectric. Electrodes are placed over a portion of the pouch on either side; when an increasing voltage (V) is applied, electrostatic forces displace the liquid dielectric, causing the electrodes to progressively close. This forces fluid into the uncovered portion of the pouch, causing a transition from a flat cross section to a more circular one, which leads to a contractile force, F . (B) Schematic side view of a three-unit Peano-HASEL actuator with voltage off and voltage on. The theoretical maximum strain for the contracting area of the pouch is $1 - \frac{2}{\pi}$ or about 36%. L_0 , length of contracting area with voltage off. L , length of contracting area with voltage on. (C) Three-unit Peano-HASEL actuator shown lifting 20 g on application of 8 kV across the electrodes. This construction used transparent hydrogels as electrodes and fiberglass-reinforced tape for mounting connections.

of the pouch, causing this region to transition from a flat cross section toward a more circular one. Because the shell is inextensible, this transition results in linear contraction of the actuator. The theoretical maximum strain is $\sim 36\%$ ($1 - 2/\pi$) in the contracting area, as can be seen through simple geometric changes in cross section shown in Fig. 1B. For our design, only half of each pouch is contracting area, whereas the other half is reserved for electrodes, so the theoretical maximum overall strain is limited to $\sim 18\%$. Figure 1C shows a three-unit Peano-HASEL actuator with no rigid components contracting on application of 8 kV.

Fabrication of devices

Figure 2A shows the three central components used to fabricate Peano-HASEL actuators. The shell material is a biaxially oriented polypropylene (BOPP) film that is heat sealable on one side. This material is commonly used in food packaging for its mechanical strength, as well as in commercial capacitors for its high dielectric breakdown strength of ~ 700 V μm^{-1} (35). The liquid dielectric is Envirotemp FR3—a high breakdown strength vegetable-based transformer oil. Last, we use ionically conductive hydrogel electrodes (36) to provide a voltage across our actuators. These are laser cut from a polyacrylamide hydrogel swollen with an aqueous LiCl solution (37) and bonded to a thin polydimethylsiloxane (PDMS) substrate (38) for mechanical support. Figure 2 (B to F) illustrates the heat-sealing process used to construct these actuators. First, we used a heat-press (detailed in fig. S1) with a heated metal die for

sealing actuator pouches. We left gaps in the seal of each pouch to fill them with liquid dielectric. After filling, the pouches were sealed completely with a heated aluminum bar. Last, we aligned and placed the prefabricated hydrogel electrodes (described in fig. S2) on the pouches to create a completed actuator with a total weight of 5 g. We left excess BOPP on the sides of the pouches to serve as a “skirt” to prevent electrical arcing around the device during operation.

We focused on a three pouch Peano-HASEL because it allowed us to explore the behavior of connected pouches while reducing fabrication complexity. Each pouch was 4 cm wide by 2 cm high, with electrodes 3.8 cm wide by 1 cm high, covering half of the pouch height. This design made the contracting area 4 cm wide by 1 cm high; the aspect ratio 4:1 was picked to be large enough to reduce edge effects caused by the constrained sides, as found by Veale *et al.* (15) for Peano fluidic actuators. To demonstrate ease of manufacturing and compatibility with industrial production methods, we also fabricated devices with aluminum electrodes integrated on the BOPP surface using a commercial vacuum-deposition process. Our fabrication process began with metalized BOPP sheets that were etched with a KOH solution into a desired electrode pattern. The full process is detailed in fig. S3.

Force-strain characteristics

We tested the force-strain relation for two Peano-HASEL actuators—one using hydrogel electrodes and the other using aluminum electrodes.

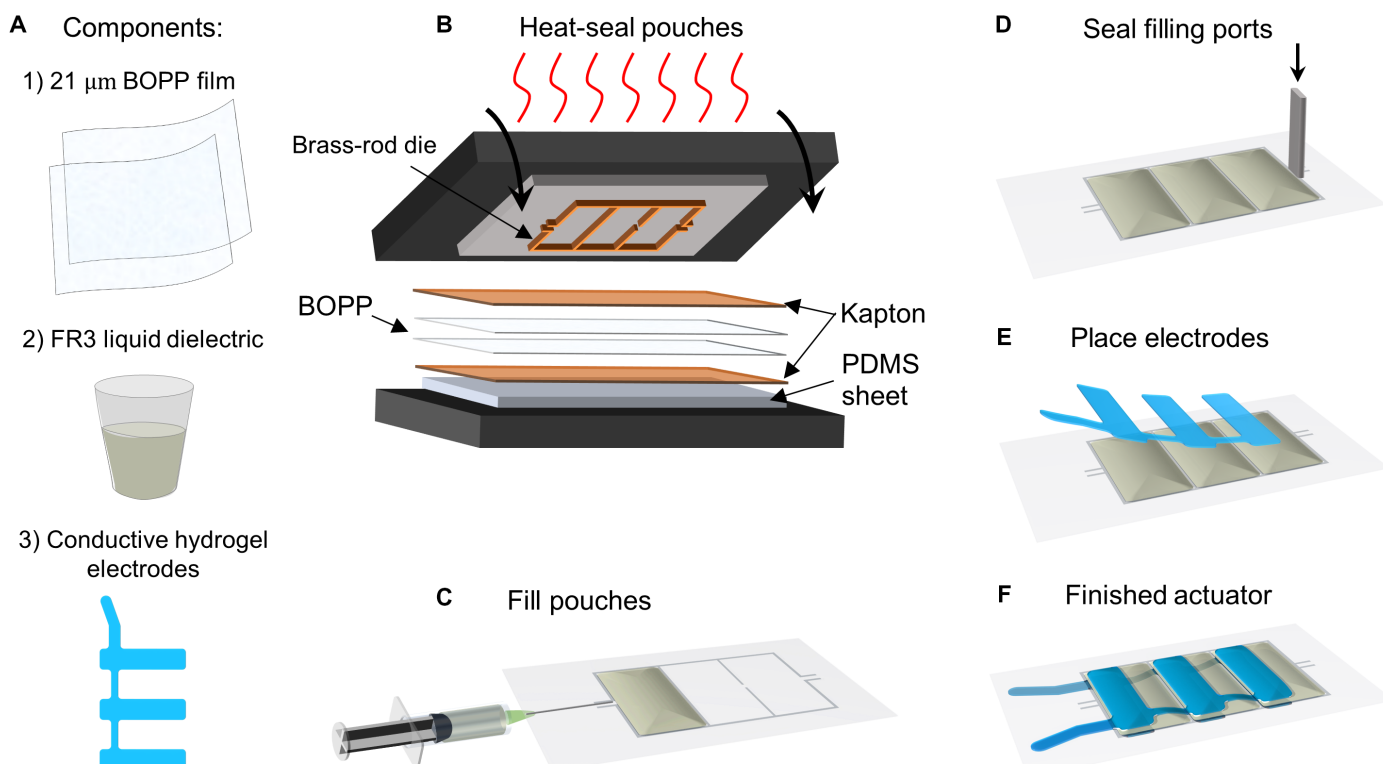


Fig. 2. Fabrication process for Peano-HASEL actuators. (A) Basic components of a Peano-HASEL actuator. (B) Two BOPP sheets were placed between two layers of Kapton film and sealed using a heated brass-rod die. The die was designed to give pouches (2 cm by 4 cm) with 2-mm access ports for filling with liquid dielectric. A PDMS sheet was placed below the Kapton as a load-dispersing layer. Figure S1 describes the heat-press in more detail. (C) Pouches were filled with FR3 liquid dielectric using a syringe. (D) A heated aluminum rod was used to seal the filling ports. (E) PDMS-backed hydrogel electrodes were placed on each side of the pouches. Figure S2 describes the process for fabricating these electrodes. (F) A finished actuator is shown.

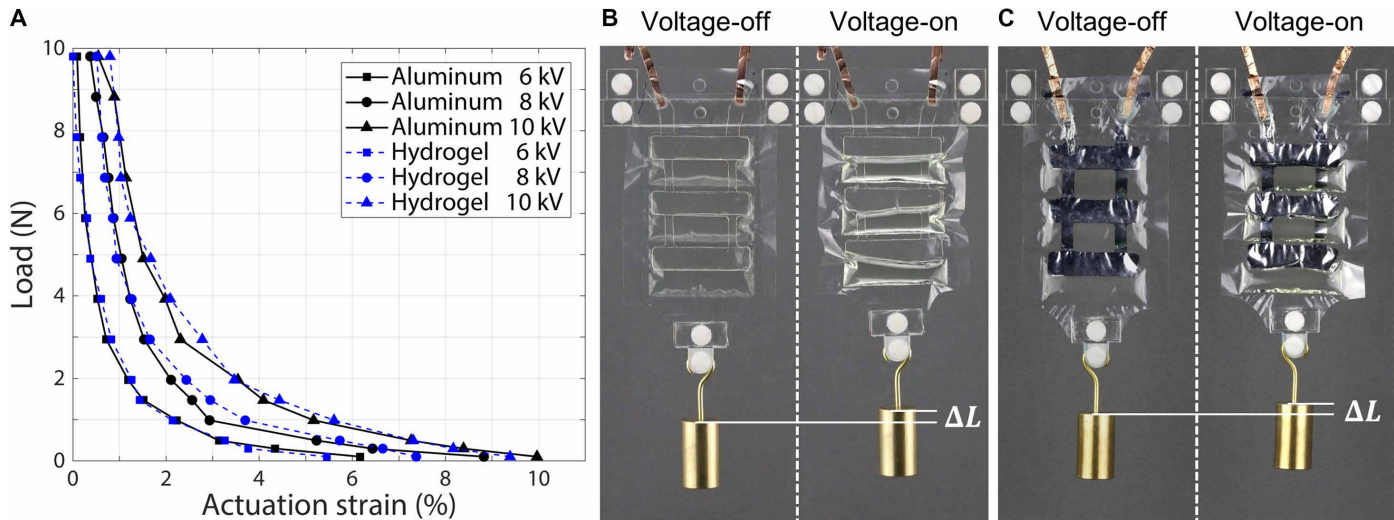


Fig. 3. Force-strain characteristics of Peano-HASEL actuators using hydrogel and aluminum electrodes. (A) Comparison of the force-strain curves for two Peano-HASEL actuators, one using hydrogel and the other using aluminum electrodes, revealing no difference in performance. A maximum of 10% strain was observed under a 20-g load at 10-kV applied voltage. (B) A hydrogel-electrode actuator was mounted on an acrylic stand for actuation tests and demonstrated contraction under 20-g load at 8 kV. (C) An aluminum-electrode actuator was mounted on an acrylic stand for actuation tests and demonstrated contraction under 20-g load at 8 kV.

A modified square-wave voltage signal with long rise and fall times (~ 1 s) was used to ensure consistent actuation (fig. S4). Actuators were tested at 6, 8, and 10 kV; this corresponded to maximum electric fields of 140, 190, and 240 V μm^{-1} , respectively. The measured force-strain curves are depicted in Fig. 3A and show no difference between aluminum- and hydrogel-electrode performance, demonstrating versatility in material selection and design. The highest load applied to the actuators was 10 N (1 kg), which corresponded to the blocking force for actuators activated at 6 kV and was less than the blocking force at 8 and 10 kV. The 1-kg load resulted in a maximum cross-sectional stress of 6 MPa in the actuator. A strain of 10% was achieved at 10 kV with a 0.02-N (20 g) load. The shape of the observed force-strain relation is characteristic of Peano-fluidic actuators (12). Furthermore, the monotonic decrease in force with strain is also observed in skeletal muscle (20).

Figure 3 (B and C) shows examples of actuators with hydrogel and aluminum electrodes, respectively. Movies S1 and S2 demonstrate the dynamics of both types of actuators. Although the vacuum-deposited aluminum electrodes show promise for industrially amenable fabrication, the very thin aluminum layers used in this paper (~ 30 nm) made the electrodes vulnerable to mechanical wear and ablation during high-voltage operation (fig. S5).

Arrays of parallel actuators for scaling up forces

A key feature of biological muscle is its massively parallelized structure, which allows for high-force generation and operational redundancy. Figure 4A demonstrates a method for efficiently stacking Peano-HASEL actuators in parallel to increase actuation force. Offsetting actuators vertically allows the expanding cross section of one actuator to nest within the pulled-in electrode area of adjacent actuators. Alternating electrode polarities ensures that adjacent electrodes are always at the same potential. Figure 4B shows a 1.4-cm-thick stack of six actuators in its inactive and active state to visualize the offset configuration. As expected, the stack demonstrated an actuation force roughly six times that of an individual Peano-HASEL actuator, as shown in Fig. 4C. Figure 4D shows this

stack, which weighs 30 g, lifting 500 g over a strain of 4.6%. Movie S3 shows several lifting cycles for this 500-g mass, as well as actuation with a filled water bottle (~ 1 kg).

High-speed actuation

For most fluidic actuators, the limiting factor in mechanical response is the time required to pump the working fluid throughout the system. Because Peano-HASELs locally pump the fluid in each pouch, we reduce the distance the fluid must travel, which reduces actuation time. In addition, we reduce viscous loss and design complexity by avoiding the need for regulators and valves.

To elucidate the fast-actuation characteristics of Peano-HASEL actuators, we examined contraction speed under an inertial load (i.e., a hanging weight), as shown in Fig. 5A. We applied a square-wave voltage signal and measured mechanical response as a function of time for loads ranging from 10 to 500 g; Fig. 5B plots actuator response for a 100-g load. Actuators took between 12 ms (for a 10-g load) and 18 ms (for a 500-g load) from initial contraction t_s to their equilibrium strain t_e as we varied the loads between 10 and 500 g. The total load is the hanging weight (e.g., 10 g) plus the mass of the lower mounting piece (4 g). Performance parameters, such as peak strain rate and specific power, were calculated between t_s and t_e . Calculations are described in the Supplementary Materials; fig. S6 (B to E) shows the data produced for a 100-g load.

Peak strain rate as a function of load is shown in Fig. 5C; we see a generally hyperbolic relation for these actuators, which resembles the force-velocity relation for mammalian muscle under isotonic contraction (39). Values varied between 140 and 8900% s^{-1} depending on the load; our maximum strain rate was nearly two times the maximum achievable strain rate in mammalian skeletal muscle (5000% s^{-1}) (40). By comparison, DEAs have demonstrated peak strain rates between 450 and 4500% s^{-1} for acrylic elastomers and up to 34,000% s^{-1} for silicone elastomers (41); however, these numbers are for radially expanding DEAs that require prestretch and do not act on external loads.

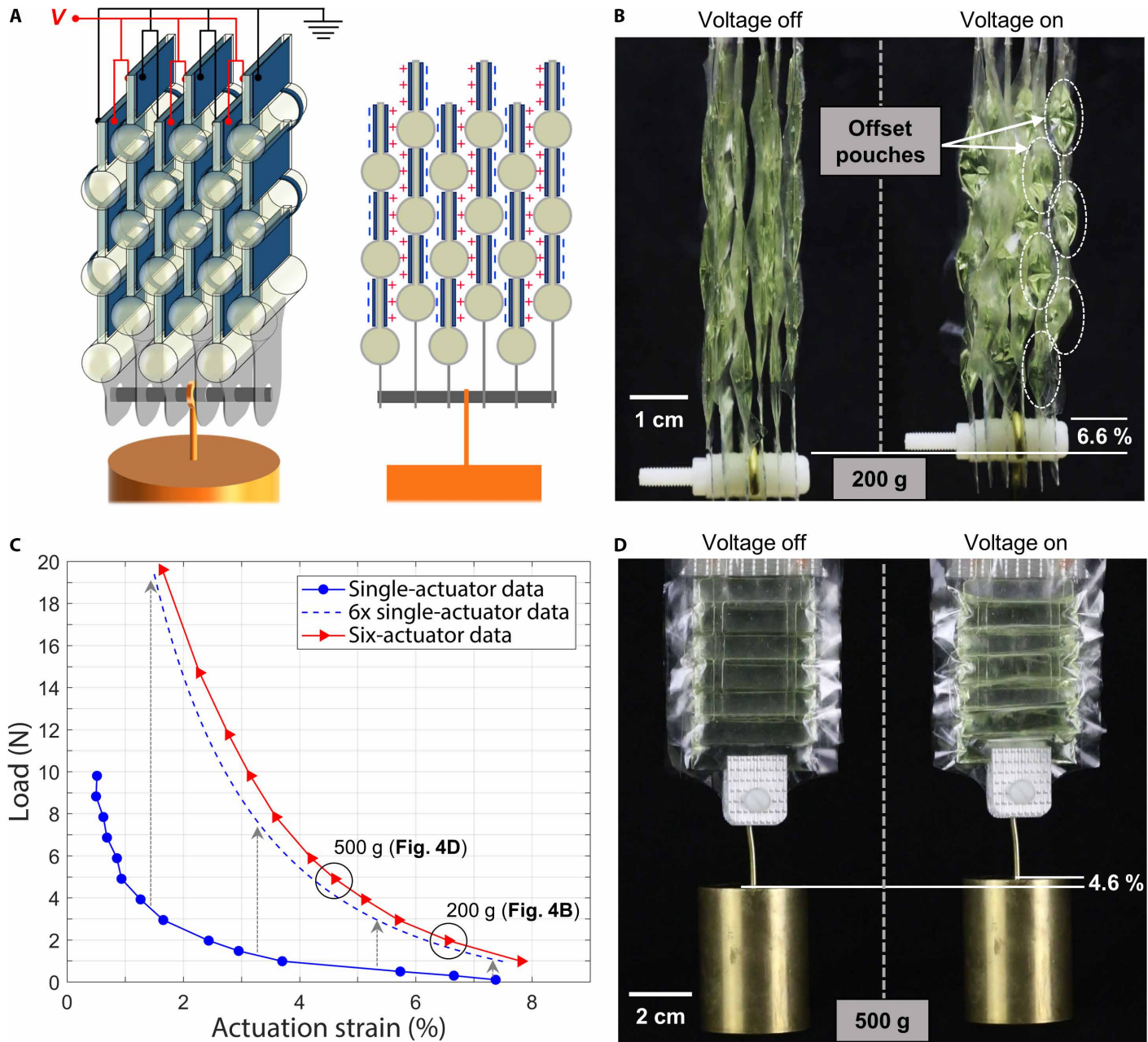


Fig. 4. Scaling up forces with arrays of Peano-HASEL actuators. **(A)** Peano-HASEL actuators arranged in parallel to scale up force generation in a compact array. Actuators are stacked such that adjacent actuators are vertically offset by half of the pouch height. Electrode polarity alternates (as shown on the right) such that electrodes facing each other from adjacent actuators are always at the same potential. **(B)** Six actuators shown contracting 6.6% under a 200-g load at 8 kV. The white ovals show the offset pouches in the two rightmost actuators. **(C)** Comparison of the force-strain characteristics for one actuator to an array of six. Single-actuator data were projected upward by multiplying the load by six (dashed line) to estimate expected performance for an array of six actuators. The array of six actuators slightly outperforms expected results, demonstrating the ability to effectively scale up actuation force. **(D)** Six actuators shown contracting 4.6% under a 500-g load at 8 kV.

Specific power was calculated during these contraction cycles and is shown in Fig. 5D. From this plot, we see that peak specific power was greatest during contraction with a 100-g load. The maximum value of 160 W kg^{-1} is comparable to mammalian skeletal muscle, which falls between 50 (typical) and 284 W kg^{-1} (maximum) (41). The average specific power during contraction was above 50 W kg^{-1} for all but the lowest load.

To further explore the fast actuation characteristics of fabricated Peano-HASEL actuators, we created a custom stand for mounting

the actuators (fig. S7A), with elastic bands to provide a nearly constant restoring force at a range of frequencies (Fig. 5E). Tests were conducted at various frequencies using a reversing-polarity square wave (fig. S7B). Actuation strain (normalized to maximum actuation at low frequency) is plotted as a function of frequency in Fig. 5F. Tests were performed with FR3 medium-viscosity liquid dielectric, as well as a low-viscosity mineral oil (Drakeol 7), to test viscosity dependence of the system. FR3 has a viscosity of 50 cSt at 40°C , whereas Drakeol 7 has a viscosity of ~ 12 cSt at 40°C . With FR3, the

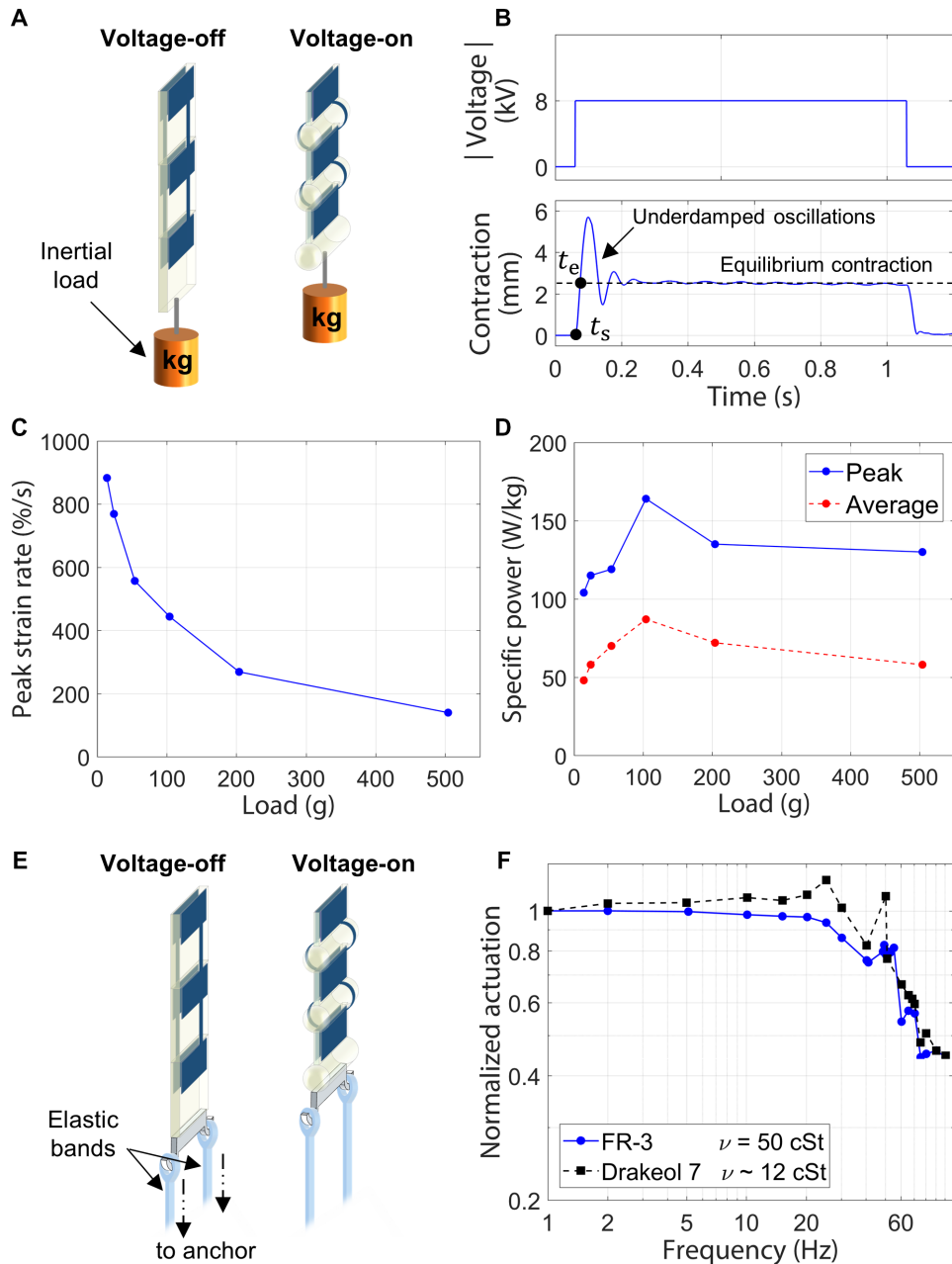


Fig. 5. High-speed performance of Peano-HASEL actuators. (A) Schematic of the test setup for determining contraction characteristics. The minimum cross section of the actuator used for testing was (40 mm by 0.042 mm) corresponding to a maximum static stress of 2.9 MPa with a 500-g load. (B) An 8-kV square wave was applied to the actuator. The resulting contraction response was measured, where t_s and t_e correspond to the time of initial contraction and equilibrium contraction, respectively. Underdamped oscillations were observed after initial contraction. The small oscillations observed after 0.3 s correspond to out-of-plane swinging of the load and are not part of the characteristic response. (C) Peak strain rate during contraction as a function of load. (D) Peak and average specific power as a function of load. (E) Schematic of the test setup for frequency response. Elastic bands were attached to the bottom of the actuator and tensioned to provide a constant 1-N restoring force. (F) Frequency response curves for Peano-HASEL actuators filled with liquid dielectrics of different viscosities. The actuator filled with FR3 liquid dielectric showed a nearly flat response up to 20 Hz. The lower viscosity Drakeol 7 allowed maximum actuation at higher frequencies.

three-unit actuator had a cutoff frequency of more than 40 Hz and actuated with >90% maximum actuation up to 25 Hz. Movie S4 shows the performance of an FR3-filled actuator at several frequencies from 1 to 50 Hz. With Drakeol 7, we see undiminished actuation up

to 30 Hz. The flat frequency profile below cutoff is attractive for simple control when used in robotic systems. Various resonance peaks can be seen in the data and are likely a result of the elastic bands used during testing. These results indicate that frequency characteristics depend on the viscosity of the liquid dielectric. Actuation speed should similarly depend on pouch geometry and size and can be improved by future optimization efforts.

Demonstration of fast and precise actuation

To illustrate fast and precisely controlled actuation of Peano-HASEL actuators in a robotic application, we constructed a 7:1 acrylic lever arm connected to two actuators in a parallel configuration (Fig. 6A) and applied a variety of voltage signals. Applying a 13-kV voltage step allowed fast contraction to throw a table tennis ball 24 cm into the air (Fig. 6B). To demonstrate controllable static displacement, voltage was increased from 1 to 12 kV in 1-kV increments, with 0.75-s hold time at each voltage, with three illustrative voltages shown in Fig. 6C. Movie S5 shows the full demonstration of actuation, which includes progressive voltage steps, sinusoidal actuation, and the 13-kV voltage step. Figure S8 shows the voltage profile used for the demonstration. The fast and controllable actuation of Peano-HASEL actuators is largely due to the near-incompressibility of liquids, which generally leads to higher bandwidth and better static position control than equivalent pneumatic systems (42).

The control of autonomous mechanical systems requires sensory feedback. Because Peano-HASEL actuators are variable capacitors, their capacitance state can provide information on their deformation state. Keplinger *et al.* (23) has shown previously that by continuously monitoring the capacitance of DEAs, one can glean information on the mechanical deformation of the system. We adopted this method for Peano-HASEL actuators, using the setup described by Acome *et al.* (29) to self-sense deformation; the basic idea relies on superimposing a low-voltage ac signal onto the high-voltage dc actuation signal and then analyzing the electrical impedance of the system. The position of the actuator was optically tracked while applying an actuation voltage signal similar to fig. S8; these data were compared to the changing capacitance signal, with the results shown in Fig. 7. Capacitance data were multiplied

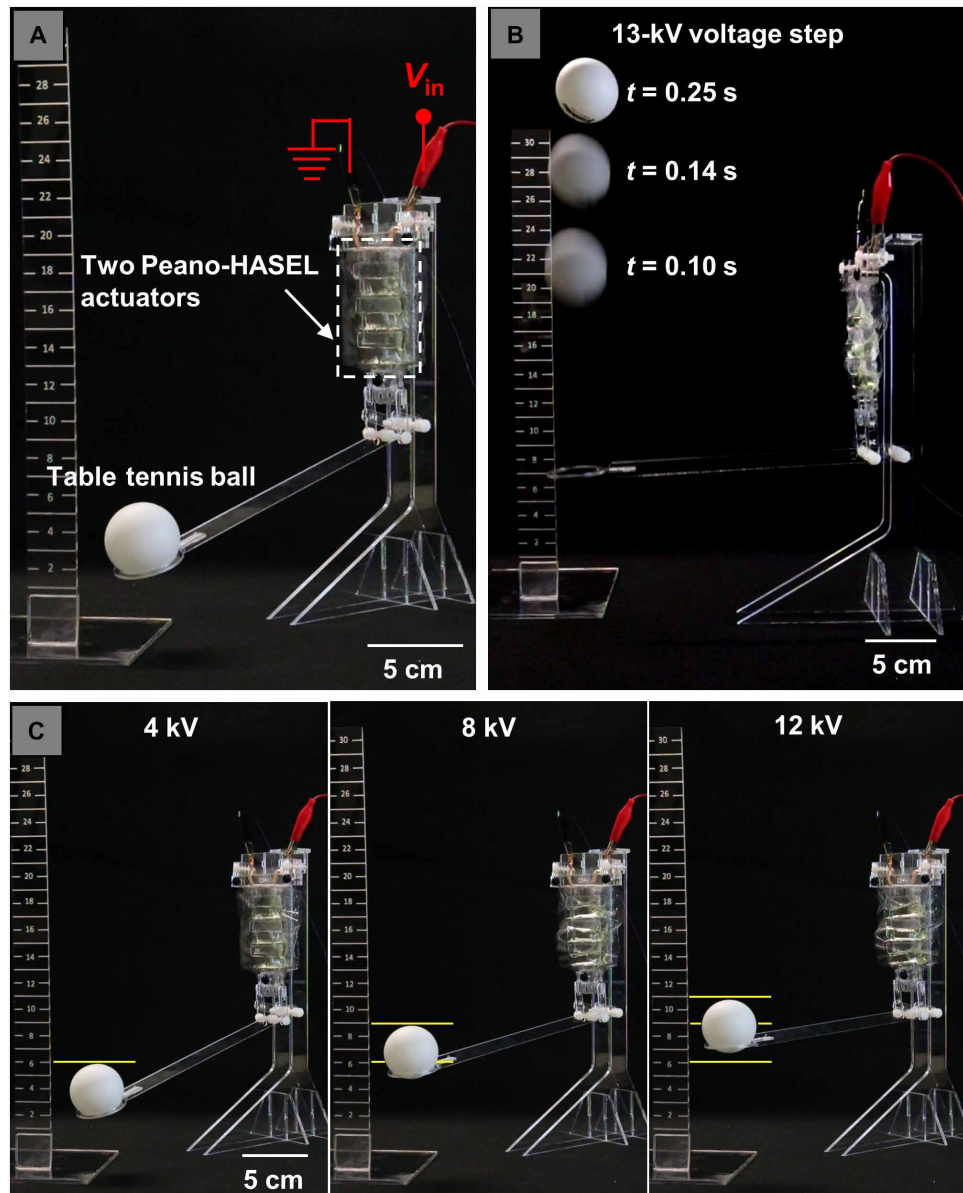


Fig. 6. Demonstration of high-speed and precise actuation. (A) A lever-arm setup was connected to two Peano-HASEL actuators in parallel for demonstrating fast and controllable actuation. (B) By applying a 13-kV voltage step, these actuators contracted fast enough to throw a ping-pong ball 24 cm into the air. Labeled times are measured from the start of contraction. (C) Incrementing voltage allowed controllable actuation of the arm, as shown in the progression of images with increasing voltage left to right. The yellow lines mark the position of the top of the ball for comparison. The ruler to the left of each picture shows 1-cm increments for scale.

by a constant scaling factor to allow comparison with the optical data. Reasonable agreement was observed between the two data sets. The observed discrepancy implies a nonlinear relationship between capacitance and strain. Experimental determination of this nonlinearity would enable calibration of capacitive data and allow for precise dynamic information on the deformation state of the actuator, mimicking the proprioceptive nature of biological systems.

An imperceptible actuator

Using BOPP films and PDMS/hydrogel electrodes allows construction of an actuator that is highly transparent when submerged in an

index-matched liquid. Figure 8A shows a Peano-HASEL actuator in air. Submersion in Drakeol 19 mineral oil (Fig. 8B) led to a substantial reduction in light dispersion and high transparency. Figure 8C shows this actuator contracting with a 10-g load. Movie S6 shows the process of submerging the actuator followed by actuation while fully submerged. Peano-HASELs have the potential to be virtually invisible and operable in water by (i) fully encapsulating and insulating the electrodes and (ii) using a liquid dielectric with an index of refraction that matches water.

Actuator lifetime

Lifetime tests were performed for two actuators—one at 6 Hz and the other at 50 Hz—with the same setup used for testing frequency response. Actuator failure occurred after ~20,000 cycles in both cases. No observable decrease in actuation was measured before electrical breakdown, which occurred through the heat seal of the actuators near the electrodes. These results are presented in fig. S9 for the 6-Hz test. Although these results are promising, actuator lifetime may be improved through optimization of materials and pouch geometries.

DISCUSSION

Here, we have introduced a class of artificial muscle actuators based on electrohydraulic operating principles. Peano-HASEL actuators are versatile and provide many muscle-mimetic properties, including contraction on activation, muscle-like specific power, and the potential for highly parallelized stacking for increased force generation. In some areas, such as peak strain rate and frequency response, they exceed the performance of mammalian skeletal muscle.

Compared with current fluidic actuators and DEAs, Peano-HASELs exhibit several promising qualities. First, Peano-

HASEL actuators linearly contract on activation without stacks, pre-stretch, or frames, which makes them unique in the field of electrostatic actuators. Second, by locally displacing liquid dielectrics, Peano-HASEL actuators reduce viscous loss within the system, increase their response speed, and achieve high positional control. Further, their flat frequency response until cutoff and minimal elasticity lead to simpler kinematics for actuator control and modeling. In addition, the ability of Peano-HASEL actuators to self-sense their deformation state through capacitance monitoring mimics the proprioceptive nature of muscle. In contrast to hydrostatically coupled DEAs, where electric fields are applied across elastomers (43), Peano-HASELs

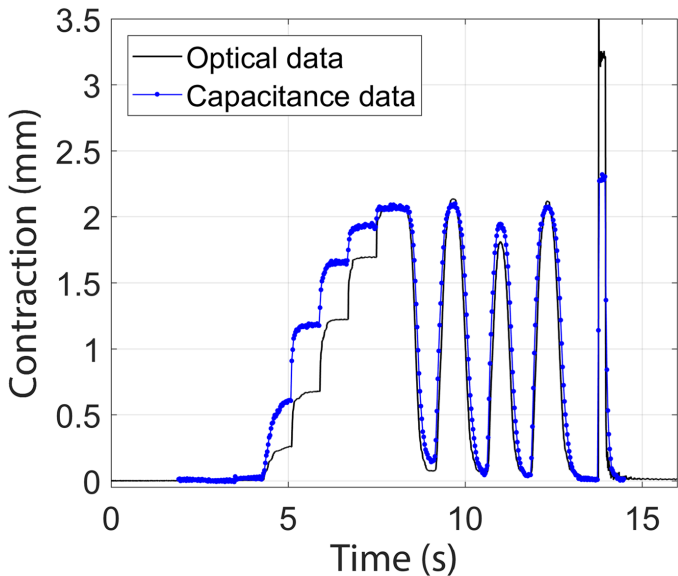


Fig. 7. Self-sensing of actuator position. Plot of dimensionless capacitance and optically tracked position data for a single actuator under the influence of a varying voltage signal. Capacitance data were multiplied by a constant scale factor to provide agreement with position data; no other calibration was performed.

apply electric fields through a deformable structure containing a liquid dielectric, which does not have to rely on highly stretchable electrodes and dielectrics. The resulting flexibility in material selection enables Peano-HASELs to be low cost, versatile, and compatible with roll-to-roll industrial fabrication processes such as heat sealing and vacuum-deposition of electrodes. Currently, hydrogel-electrode actuators can be made for $\sim \$0.10$ in materials, which should reduce considerably for large-scale fabrication. Last, actuator characteristics are largely independent of the constituent materials—assuming they meet certain criteria such as flexibility and high breakdown strength—therefore, design can be tailored for attractive properties like high transparency.

Moving forward, there are many opportunities to explore new materials, geometries, and methods of fabrication to improve performance and resolve current limitations of Peano-HASEL actuators. One outstanding issue is their inability to consistently self-heal because of the thin BOPP layer, which can puncture after dielectric breakdown events, allowing fluid to leak out. With next-generation materials, these actuators should achieve the same self-healing properties shown by Acome *et al.* (29) for HASEL actuators. An existing hurdle for electrostatic actuators is the requirement of high electric fields, which typically means providing voltages of several kilovolts. Operational voltages can be reduced by improving the design of actuators through the use of dielectrics with high permittivity, reducing the thickness of dielectric layers and exploring alternate geometries. However, there are already several commercial options for supplying and controlling high voltage that are readily available: XP Power and Pico Electronics produce several ultraminiature high-voltage dc-dc converters that can produce up to 10 kV using a 5-V input; IXYS manufactures metal oxide semiconductor field-effect transistors, and Voltage Multipliers Inc. produces optocouplers for fast switching of high-voltage signals. In addition, several groups have created their own high-voltage control systems (44–46). As it stands, the combination of properties for Peano-HASEL actuators

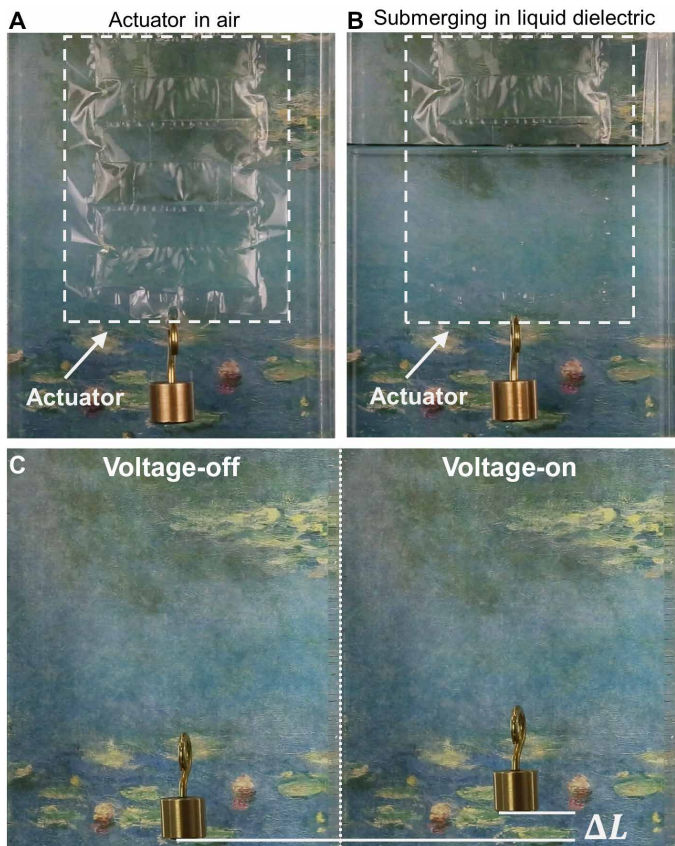


Fig. 8. Invisible Peano-HASEL actuators. (A) A Peano-HASEL actuator was suspended in an acrylic box with a colorful background (Claude Monet's Water Lilies). (B) The acrylic box was filled with a liquid dielectric (Drakeol 19). The submerged portion of the actuator is nearly invisible. (C) Submerged actuator with a suspended 10-g weight and no applied voltage. On application of 8 kV, the actuator contracted and lifted the weight.

shown in this study highlights their promise for next-generation soft robotic systems.

MATERIALS AND METHODS

Actuator materials

The inextensible shell was made from one-side metallized, one-side heat sealable, 21- μm BOPP obtained from Impex Global (MSB 20 film). Measurements confirmed the dielectric breakdown strength of our BOPP film to be $\geq 650 \text{ V } \mu\text{m}^{-1}$ (as shown in fig. S10) after our KOH etch, which was in agreement with the literature value (35). Our liquid dielectric was Envirotemp FR3 transformer oil, which was purchased from Cargill. As stated, two types of electrodes were tested: Aluminum electrodes were made during manufacture of the BOPP film through a vacuum-deposition process; hydrogel electrodes were prepared according to Keplinger *et al.* (36) and Bai *et al.* (37) and bonded to a PDMS backing. To promote strong bonding between the hydrogel and PDMS backing, we applied a benzophenone treatment to the PDMS (38), as described in the Supplementary Materials.

We used two methods to mount actuators for testing. The first consisted of fiberglass-reinforced packaging tape (pictured in Fig. 1C) for an actuator design with no rigid components. The second used

acrylic frames to provide a consistent mounting position and load-bearing points.

Testing methods

For actuation tests, frequency tests, and contraction speed tests, contraction was measured with Tracker video analysis software (version 4.96). All tests used reversing-polarity voltage signals to minimize what appeared to be charge accumulation on the BOPP actuators. These signals were generated using custom LabVIEW VIs (version 15.0.1f2) and fed into a Trek Model 50/12 high-voltage amplifier through an NI 6212 data acquisition system (DAQ). Low-speed tests used a Canon EOS 6D DSLR camera to provide data for optical tracking, whereas high-speed tests (frequency and contraction speed) used a Vision Research Phantom v710 high-speed camera. More detail on actuator materials, fabrication, and testing methods may be found in the Supplementary Materials.

SUPPLEMENTARY MATERIALS

robotics.sciencemag.org/cgi/content/full/3/14/eaar3276/DC1

Materials and Methods

Fig. S1. Heat-press used for sealing BOPP pouches.

Fig. S2. Fabrication process for Peano-HASEL actuators with hydrogel electrodes.

Fig. S3. Fabrication process for Peano-HASEL actuators with aluminum electrodes.

Fig. S4. Voltage signal with reversing polarity used during force-strain tests.

Fig. S5. Example of damage to aluminum electrodes after voltage cycling.

Fig. S6. High-speed contraction of Peano-HASEL actuators.

Fig. S7. Experimental setup used for frequency response tests of Peano-HASEL actuators.

Fig. S8. Full actuation signal for lever arm tests.

Fig. S9. Lifetime test for Peano-HASEL actuators.

Fig. S10. Dielectric breakdown tests for KOH-etched BOPP film.

Movie S1. Demonstration of actuation characteristics.

Movie S2. Actuation using integrated aluminum electrodes.

Movie S3. Scaling up forces with Peano-HASEL actuators.

Movie S4. Frequency response of Peano-HASEL actuators.

Movie S5. Demonstration of precise and rapid actuation.

Movie S6. Transparent Peano-HASEL actuators.

References (47, 48)

REFERENCES AND NOTES

1. E. W. Hawkes, L. H. Blumenschein, J. D. Greer, A. M. Okamura, A soft robot that navigates its environment through growth. *Sci. Robot.* **2**, eaan3028 (2017).
2. M. T. Tolley, R. F. Shepherd, B. Mosadegh, K. C. Galloway, M. Wehner, M. Karpelson, R. J. Wood, G. M. Whitesides, A resilient, untethered soft robot. *Soft Robot.* **1**, 213–223 (2014).
3. H. Yuk, S. Lin, C. Ma, M. Takaffoli, N. X. Fang, X. Zhao, Hydraulic hydrogel actuators and robots optically and sonically camouflaged in water. *Nat. Commun.* **8**, 14230 (2017).
4. C. Larson, B. Peele, S. Li, S. Robinson, M. Totaro, L. Beccai, B. Mazzolai, R. Shepherd, Highly stretchable electroluminescent skin for optical signaling and tactile sensing. *Science* **351**, 1071–1074 (2016).
5. S. Kim, C. Laschi, B. Trimmer, Soft robotics: A bioinspired evolution in robotics. *Trends Biotechnol.* **31**, 287–294 (2013).
6. Y. Cao, T. G. Morrissey, E. Acome, S. I. Allec, B. M. Wong, C. Keplinger, C. Wang, A transparent, self-healing, highly stretchable ionic conductor. *Adv. Mater.* **29**, 1605099 (2017).
7. L. Hines, K. Petersen, G. Z. Lum, M. Sitti, Soft actuators for small-scale robotics. *Adv. Mater.* **29**, 1603483 (2017).
8. C. S. Haines, M. D. Lima, N. Li, G. M. Spinks, J. Foroughi, J. D. W. Madden, S. H. Kim, S. Fang, M. J. de Andrade, F. Göktepe, Ö. Göktepe, S. M. Mirvakili, S. Naficy, X. Lepró, J. Oh, M. E. Kozlov, S. J. Kim, X. Xu, B. J. Swedlove, G. G. Wallace, R. H. Baughman, Artificial muscles from fishing line and sewing thread. *Science* **343**, 868–872 (2014).
9. F. Ilievski, A. D. Mazzeo, R. F. Shepherd, X. Chen, G. M. Whitesides, Soft robotics for chemists. *Angew. Chem. Int. Ed.* **123**, 1930–1935 (2011).
10. D. Yang, M. S. Verma, J.-H. So, B. Mosadegh, C. Keplinger, B. Lee, F. Khashai, E. Lossner, Z. Suo, G. M. Whitesides, Buckling pneumatic linear actuators inspired by muscle. *Adv. Mater. Technol.* **1**, 1600055 (2016).
11. M. A. Meller, M. Bryant, E. Garcia, Reconsidering the McKibben muscle: Energetics, operating fluid, and bladder material. *J. Intell. Mater. Syst. Struct.* **25**, 2276–2293 (2014).
12. R. Niyyama, D. Rus, S. Kim, Pouch motors: Printable/inflatable soft actuators for robotics, in *Proceedings of the 2014 IEEE International Conference on Robotics and Automation (ICRA)* (IEEE, 2014), pp. 6332–6337.
13. S. Sanan, P. S. Lynn, S. T. Griffith, Pneumatic torsional actuators for inflatable robots. *J. Mech. Robot.* **6**, 031003 (2014).
14. A. J. Veale, I. A. Anderson, S. Q. Xie, The smart Peano fluidic muscle: A low profile flexible orthosis actuator that feels pain. *Proc. SPIE* **9435**, 94351V (2015).
15. A. J. Veale, S. Q. Xie, I. A. Anderson, Characterizing the Peano fluidic muscle and the effects of its geometry properties on its behavior. *Smart Mater. Struct.* **25**, 065013 (2016).
16. R. Pelrine, R. D. Kornbluh, Q. Pei, J. Joseph, High-speed electrically actuated elastomers with strain greater than 100%. *Science* **287**, 836–839 (2000).
17. P. Brochu, Q. Pei, Advances in dielectric elastomers for actuators and artificial muscles. *Macromol. Rapid Commun.* **31**, 10–36 (2010).
18. S. Rosset, H. R. Shea, Small, fast, and tough: Shrinking down integrated elastomer transducers. *Appl. Phys. Rev.* **3**, 031105 (2016).
19. G.-Y. Gu, J. Zhu, L.-M. Zhu, X. Zhu, A survey on dielectric elastomer actuators for soft robots. *Bioinspir. Biomim.* **12**, 011003 (2017).
20. F. Daerden, D. Lefeber, Pneumatic artificial muscles: Actuators for robotics and automation. *Eur. J. Mech. Environ. Eng.* **47**, 11–21 (2002).
21. P. Polygerinos, N. Correll, S. A. Morin, B. Mosadegh, C. D. Onal, K. Petersen, M. Cianchetti, M. T. Tolley, R. F. Shepherd, Soft robotics: Review of fluid-driven intrinsically soft devices; manufacturing, sensing, control, and applications in human-robot interaction. *Adv. Eng. Mater.* **19**, 1700016 (2017).
22. M. Wehner, R. L. Truby, D. J. Fitzgerald, B. Mosadegh, G. M. Whitesides, J. A. Lewis, R. J. Wood, An integrated design and fabrication strategy for entirely soft, autonomous robots. *Nature* **536**, 451–455 (2016).
23. C. Keplinger, M. Kaltenbrunner, N. Arnold, S. Bauer, Capacitive extensometry for transient strain analysis of dielectric elastomer actuators. *Appl. Phys. Lett.* **92**, 192903 (2008).
24. S. Diaham, S. Zelmat, M.-L Locatelli, S. Dinculescu, M. Decup, T. Lebey, Dielectric breakdown of polyimide films: Area, thickness and temperature dependence. *IEEE Trans. Dielectr. Electr. Insul.* **17**, 18–27 (2010).
25. M. Duduta, R. J. Wood, D. R. Clarke, Multilayer dielectric elastomers for fast, programmable actuation without prestretch. *Adv. Mater.* **28**, 8058–8063 (2016).
26. M. Vatankhah-Varnoosfaderani, W. F. M. Daniel, A. P. Zhushma, Q. Li, B. J. Morgan, K. Matyjaszewski, D. P. Armstrong, R. J. Spontak, A. V. Dobrynin, S. S. Sheiko, Bottlebrush elastomers: A new platform for freestanding electroactuation. *Adv. Mater.* **29**, 1604209 (2017).
27. X. Niu, H. Stoyanov, W. Hu, R. Leo, P. Brochu, Q. Pei, Synthesizing a new dielectric elastomer exhibiting large actuation strain and suppressed electromechanical instability without prestretching. *J. Polym. Sci. Part B Polym. Phys.* **51**, 197–206 (2013).
28. G. Kovacs, L. Düring, S. Michel, G. Terrasi, Stacked dielectric elastomer actuator for tensile force transmission. *Sens. Actuators A* **155**, 299–307 (2009).
29. E. Acome, S. K. Mitchell, T. G. Morrissey, M. B. Emmett, C. Benjamin, M. King, M. Radakovitz, C. Keplinger, Hydraulically amplified self-healing electrostatic actuators with muscle-like performance. *Science* **359**, 61–65 (2018).
30. L. Maffli, S. Rosset, H. R. Shea, Zipping dielectric elastomer actuators: Characterization, design and modeling. *Smart Mater. Struct.* **22**, 104013 (2013).
31. A. S. Chen, H. Zhu, Y. Li, L. Hu, S. Bergbreiter, A paper-based electrostatic zipper actuator for printable robots, in *Proceedings of the 2014 IEEE International Conference on Robotics and Automation (ICRA)* (IEEE, 2014), pp. 5038–5043.
32. M. P. Brenner, J. H. Lang, J. Li, A. H. Slocum, Optimum design of an electrostatic zipper actuator. *NSI Nanotech 2004* **2**, 371–374 (2004).
33. A. A. Sathe, E. A. Groll, S. V. Garimella, Analytical model for an electrostatically actuated miniature diaphragm compressor. *J. Micromech. Microeng.* **18**, 035010 (2008).
34. Z. Suo, Theory of dielectric elastomers. *Acta Mech. Sol. Sin.* **23**, 549–578 (2010).
35. J. Ho, R. Jow, *Characterization of high temperature polymer thin films for power conditioning capacitors* (No. ARL-TR-4880, Army Research Laboratories, 2009).
36. C. Keplinger, J.-Y. Sun, C. C. Foo, P. Rothemund, G. M. Whitesides, Stretchable, transparent, ionic conductors. *Science* **341**, 984–987 (2013).
37. Y. Bai, B. Chen, F. Xiang, J. Zhou, H. Wang, Z. Suo, Transparent hydrogel with enhanced water retention capacity by introducing highly hydratable salt. *Appl. Phys. Lett.* **105**, 151903 (2014).
38. H. Yuk, T. Zhang, G. A. Parada, X. Liu, X. Zhao, Skin-inspired hydrogel–elastomer hybrids with robust interfaces and functional microstructures. *Nat. Commun.* **7**, 12028 (2016).
39. A. V. Hill, The heat of shortening and the dynamic constants of muscle. *Proc. R. Soc. B Biol. Sci.* **126**, 136–195 (1938).
40. I. W. Hunter, S. Lafontaine, A comparison of muscle with artificial actuators, in *Proceedings of the IEEE 5th Technical Digest, Solid-State Sensor and Actuator Workshop* (IEEE, 1992), pp. 178–185.
41. J. D. W. Madden, N. A. Vandesteeg, P. A. Anquetil, P. G. A. Madden, A. Takshi, R. Z. Pytel, S. R. Lafontaine, P. A. Wieringa, I. W. Hunter, Artificial muscle technology: Physical principles and naval prospects. *IEEE J. Ocean. Eng.* **29**, 706–728 (2004).

42. M. Focchi, E. Guglielmino, C. Semini, A. Parmiggiani, N. Tsagarakis, B. Vanderborght, D. G. Caldwell, Water/air performance analysis of a fluidic muscle, in *Proceedings of IEEE/RSJ 2010 International Conference on Intelligent Robots and Systems (IROS)* (IEEE, 2010), pp. 2194–2199.
43. F. Carpi, G. Frediani, D. De Rossi, Hydrostatically coupled dielectric elastomer actuators. *IEEE/ASME Trans. Mech.* **15**, 308–315 (2010).
44. T. Li, G. Li, Y. Liang, T. Cheng, J. Dai, X. Yang, B. Liu, Z. Zeng, Y. Luo, T. Xie, W. Yang, Fast-moving soft electronic fish. *Sci. Adv.* **3**, e1602045 (2017).
45. B. M. O'Brien, E. P. Calius, T. Inamura, S. Q. Xie, I. A. Anderson, Dielectric elastomer switches for smart artificial muscles. *Appl. Phys. A* **100**, 385–389 (2010).
46. A. Marette, A. Poulin, N. Basse, S. Rosset, D. Briand, H. Shea, Flexible zinc-tin oxide thin film transistors operating at 1 kV for integrated switching of dielectric elastomer actuators arrays. *Adv. Mater.* **29**, 1700880 (2017).
47. E. M. Mount III, C. A. Bishop, Figure 2.2.1 in *Metallizing Technical Reference* (Association of International Metallizers, Coaters and Laminators, 2012).
48. Impex Global, *Metallized BOPP Film* (Technical Data Sheet); www.impexfilms.com/wp-content/uploads/2017/01/63_2METOPP70-120.pdf.

Acknowledgments: We thank S. Humbert for the use of high-speed camera equipment (Phantom v710 and high-power tungsten flood lights). Special thanks to Impex Global for providing samples of BOPP film and to Penreco for providing samples of Drakeol 7 and Drakeol 19 mineral oil for actuator construction and testing. **Funding:** This work was sponsored by start-up funds from the University of Colorado Boulder. G.M.S. acknowledges financial support from the Undergraduate Research Opportunity Program at the University of

Colorado Boulder. **Author contributions:** C.K. conceived and supervised the research. N.K., V.G.V., and S.K.M. designed the Peano-HASEL actuators. N.K. and V.G.V. developed fabrication methods for actuators. G.M.S., V.G.V., and N.K. fabricated actuators. N.K., V.G.V., and G.M.S. designed experiments/demos and collected data. S.K.M. performed dielectric breakdown tests on BOPP. V.G.V. and N.K. analyzed data from force-strain tests and high-speed video for frequency and contraction tests. N.K. designed and revised supplementary and main text figures with contributions from all authors. G.M.S. designed and revised supplementary videos. V.G.V. drafted and revised supplemental text. N.K., C.K., V.G.V., and S.K.M. drafted and revised the manuscript with contributions from G.M.S.

Competing interests: The authors declare that they have no competing financial interests. N.K., S.K.M., and C.K. are listed as inventors on a U.S. provisional patent application (62/474,814) submitted by the University of Colorado Boulder that covers fundamental principles and designs of Peano-HASEL actuators. **Data and materials availability:** All data needed to support the conclusions of this manuscript are included in the main text or supplementary materials. Contact C.K. for materials.

Submitted 2 November 2017

Accepted 20 December 2017

Published 5 January 2018

10.1126/scirobotics.aar3276

Citation: N. Kellaris, V. Gopaluni Venkata, G. M. Smith, S. K. Mitchell, C. Keplinger, Peano-HASEL actuators: Muscle-mimetic, electrohydraulic transducers that linearly contract on activation. *Sci. Robot.* **3**, eaar3276 (2018).

Science Robotics

Peano-HASEL actuators: Muscle-mimetic, electrohydraulic transducers that linearly contract on activation

Nicholas Kellaris, Vidyacharan Gopaluni Venkata, Garrett M. Smith, Shane K. Mitchell and Christoph Keplinger

Sci. Robotics **3**, eaar3276.
DOI: 10.1126/scirobotics.aar3276

ARTICLE TOOLS

<http://robotics.sciencemag.org/content/3/14/eaar3276>

SUPPLEMENTARY MATERIALS

<http://robotics.sciencemag.org/content/suppl/2018/01/02/3.14.eaar3276.DC1>

RELATED CONTENT

<http://science.sciencemag.org/content/sci/359/6371/61.full>
<http://robotics.sciencemag.org/content/robotics/5/41/eaaz4239.full>

REFERENCES

This article cites 41 articles, 6 of which you can access for free
<http://robotics.sciencemag.org/content/3/14/eaar3276#BIBL>

PERMISSIONS

<http://www.sciencemag.org/help/reprints-and-permissions>

Use of this article is subject to the [Terms of Service](#)

Science Robotics (ISSN 2470-9476) is published by the American Association for the Advancement of Science, 1200 New York Avenue NW, Washington, DC 20005. The title *Science Robotics* is a registered trademark of AAAS.

Copyright © 2018 The Authors, some rights reserved; exclusive licensee American Association for the Advancement of Science. No claim to original U.S. Government Works